


Maximizing the relationship of yield to site-specific management zones with object-oriented segmentation of hyperspectral images

Huanjun Liu¹  · Michael L. Whiting² · Susan L. Ustin² ·
P. J. Zarco-Tejada³ · Ted Huffman⁴ · Xinle Zhang¹

© Springer Science+Business Media New York 2017

Abstract Quick and low cost delineation of site-specific management zones (SSMZ) would improve applications of precision agriculture. In this study, a new method for delineating SSMZ using object-oriented segmentation of airborne imagery was demonstrated. Three remote sensing domains—spectral, spatial, and temporal— are exploited to improve the SSMZ relationship to yield. Common vegetation indices (VI), and first and second derivatives (ρ' , ρ'') from twelve airborne hyperspectral images of a cotton field for one season ρ' were used as input layers for object-oriented segmentation. The optimal combination of VI, SSMZ size and crop phenological stage were used as input variables for SSMZ delineation, determined by maximizing the correlation to segmented yield monitor maps. Combining narrow band vegetation indices and object-oriented segmentation provided higher correlation between VI and yield at SSMZ scale than that at pixel scale by reducing multi-resource data noise. VI performance varied during the cotton growing season, providing better SSMZ delineation at the beginning and middle of the season (days after planting (DAP) 66–143). The optimal scale determined for SSMZ delineation was approximately 240 polygons for the study field, but the method also provided flexibility enabling the setting of practical scales for a given field. For a defined scale, the optimal

✉ Susan L. Ustin
slustin@ucdavis.edu

Huanjun Liu
huanjunliu@gmail.com

¹ College of Natural Resources and the Environment, Northeast Agricultural University, Harbin 150030, China

² Department of Land, Air, and Water Resources, Center for Spatial Technologies and Remote Sensing (CSTARS), University of California, Davis, 139 Veihmeyer Hall/One Shields Avenue, Davis, CA 95616-8617, USA

³ Instituto de Agricultura Sostenible (IAS), Consejo Superior de Investigaciones Científicas CSIC), Alameda del Obispo s/n, 14004 Cordoba, Spain

⁴ Agriculture and Agri-Food Canada, Eastern Cereal and Oilseed Research Centre, 960 Carling Avenue, Ottawa, ON K1A 0C6, Canada

single phenological stage for the study field was near July 11 (DAP 87) early in the growing season. SSMZs determined from multispectral VIs at a single stage were also satisfactory; compared to hyperspectral indices, temporal resolution of multi-spectral data seems more important for SSMZ delineation.

Keywords Site-specific management zone · Object-oriented segmentation · Scale · Hyperspectral remote sensing · Yield prediction · Vegetation indices

Introduction

Limited resources, serious environmental problems and the increasing demands of human population require that Earth resources are managed more judiciously. Precision agriculture proposes to optimize input use efficiency by site-specific application of nutrients and pesticides on small, within-field management zones of more homogeneous soil properties and crop growth conditions (Zhang et al. 2002). Within-field management zones are defined as site-specific management zones (SSMZs) (Davatgar et al. 2012) or site-specific management units (SSMUs) (López-Lozano et al. 2010), and there has been extensive study regarding the delineation of the spatial units using various approaches. Many studies have analyzed spatial patterns of soil properties derived from field grid sampling (Franzen et al. 2002) or mobile sensors (Johnson et al. 2003) to delineate SSMZ with geostatistical and fuzzy set clustering. The primary weakness of point sampling techniques is in the generalization of individual data points to define spatial variability in an effort to reduce the expense of collecting large numbers of sample points (Senay et al. 1998). In addition, a common disadvantage is the tendency to focus on one or two soil properties, without regard for the variability of other characteristics that potentially influence SSMZ delineation, such as soil electrical conductivity (Li et al. 2007; Moral et al. 2010; Scudiero et al. 2013). However, crop growth and yield are not determined solely by soil biophysical or chemical properties; they are also influenced by topography, local hydrology and micro-meteorology. Since crop vigor is often the best indicator of yield, imagery obtained during the growing season provides a valuable tool for including multiple factors in SSMZ delineation. The development of tractor- and harvester-mounted GPS and yield monitors brought additional tools for mapping crop yield and defining SSMZs (Simbahan et al. 2004; Diker et al. 2004). SSMZs from yield maps highlight the accumulative effect of abiotic stress on crops and identify areas which may require differential management. However, the final yield map does not, per se, provide detailed information on the factors which are contributing significantly to any heterogeneous distribution of crop yield. The yield data is also gathered at the end of the season after any potential management intervention opportunities. In-season, multi-temporal remote sensing images may be useful in identifying areas of production difference for detailed investigation during the growing season.

There is a growing demand for rapid, non-invasive acquisition of fine-scale information on soil and plant variation for site-specific management (De Benedetto et al. 2013). Both aircraft- and satellite-based remote sensing (RS) provide raster maps built on analysis of contiguous pixels rather than a distributed group of points (McBratney et al. 2003). Timely aircraft sensor images have a unique role for within-season crop and soil spatio-temporal analysis and time-critical crop management (Moran et al. 1997; Hbirkou et al. 2012), and

use has steadily increased over the past decade (Yang et al. 2009; Zarco-Tejada et al. 2005; Uno et al. 2005). De Benedetto et al. (2013) identified homogenous areas within commercial fields using a single mid-season WorldView-2 multispectral satellite image. López-Lozano et al. (2010) used Quickbird imagery to estimate LAI and integrated it with yield and soil property maps to define SSMU within a commercial maize site. For additional papers describing SSMZs with RS imagery, directly or indirectly, readers should refer to López-Lozano et al. (2010), Liu et al. (2005) and Boydell and McBratney (2002). Overall, remote sensing image data and spatial statistical methods can provide valuable and comprehensive information for site-specific management (Lan et al. 2010).

The field of image classification is experiencing a paradigm shift from pixel-based to object-oriented (OO) image analysis techniques (Gamanya et al. 2009). As the spatial resolution of remote sensing data increases, the so-called “salt-and-pepper” problem of pixel-based classification becomes more serious. This limitation has facilitated the emergence of OO classification of high spatial resolution images (Ouyang et al. 2011). Numerous published empirical studies reviewed by Blaschke and Strobl (2001) show sufficient evidence of the advantages of OO classification over pixel-based classification. The basic processing units of OO image analysis are clusters of similar pixels, known as image objects. Farming practices and environmental studies are often conducted not on individual pixels, but on defined zones that can be delimited by combining spectral, spatial and temporal information together into image objects. OO analysis provides meaningful statistics and texture calculations, increases uncorrelated feature space involving shapes (e.g. length and number of edges) and topological features (neighbors and super-objects), and improves the relationship between real-world and image objects (Benz et al. 2004).

In past studies using hyperspectral imagery (HSI), more attention was paid to spectral information rather than spatial information. Subsequently, spectral analysis methods to monitor soil and vegetation biophysico-chemical properties were developed without regard to spatial context and the potential advantages of combined spatial and spectral synergy. Also, previous OO investigations concentrated on segmenting mainly high spatial resolution broad-band images, such as IKONOS (GeoEye, Dulles, VA, USA) and QuickBird (DigitalGlobe, Longmont, C), USA), thus missing potential hyperspectral and temporal information (Johansen et al. 2007; Van Coillie et al. 2007). Combining high spatial and spectral resolution, HSI provides increased information over that available from either separately, and holds promise for the development of powerful tools in the modern RS arena (Ben-Dor et al. 2009). With the addition of frequent acquisitions, HSI completes the temporal-spatial-spectral domain. This image mapping contains spectroscopy for soil and vegetation variation, spatial context of similarity among pixels, and a temporal view of growth variation. Hence HSI can exploit methods of temporal, spatial and spectral analysis required to advance soil and vegetation spectroscopy (Ben-Dor et al. 2009).

To demonstrate this multi-domain mapping concept, a set of repeated hyperspectral images of high spatial resolution (1 m) were acquired of a cotton field and classified using OO segmentation to delineate SSMZs. The objectives of this study were to: (1) incorporate hyperspectral and multi-temporal data with OO segmentation to emphasize spatial delineation of SSMZ; (2) compare the performance of hyperspectral derivatives and multi-spectral VIs; and (3) determine the optimal VIs, segmentation scale and period of growing season for SSMZ delineation.

Materials and methods

Study area

The study area, located on the western side of the southern San Joaquin Valley of California, USA, is well known as a top producer of cotton (*Gossypium* sp.), garlic (*Allium sativum* L.), tomato (*Lycopersicon esculentum* Mill.), almonds (*Prunus dulcis*), pistachio (*Pistacia vera* L.) and alfalfa hay (*Medicago sativa* L.), as well as many grain and other crops. The site was a NASA/USDA Ag20/20 Demonstration Precision Agriculture research site, located near the city of Lemoore in Kings County (Zarco-Tejada et al. 2005), (Fig. 1a). An upland Alcala cotton (*Gossypium hirsutum*) field located at (W119.941°, N36.218°), approximately 84 ha (800 m by 800 m, Fig. 1b), was selected for study because of availability of multi-date images, and yield and management records. The field soils are clay loam over coarse-loamy, mixed (calcareous), thermic Typic Torriorthents and fine, montmorillonitic, thermic Typic Natragrids. The soils are very deep, well-drained to moderately well-drained with regions of very slow and moderately slow permeability effecting localized areas with saline and saline-sodic surface due to poor drainage and high water table (USDA-NRCS 1978).

Hyperspectral airborne acquisitions

Twelve images were acquired with the Airborne Visible Near InfraRed (AVNIR) hyperspectral sensor (OKSI, Inc. Torrance, CA, USA) during the USDA-NRCS 1978 growing season; dates and corresponding days after planting (DAP) are listed in Table 1. The sensor has 12-bit digitization over a spectral range of 430–1012 nm with 60 bands of a 9.7 nm full width half maximum slit. The study images were acquired at 1500 m above ground level for a nominal 1 m ground spatial distance. Images were pre-processed with atmospheric and geo-position calibration as described in Zarco-Tejada et al. (2005).

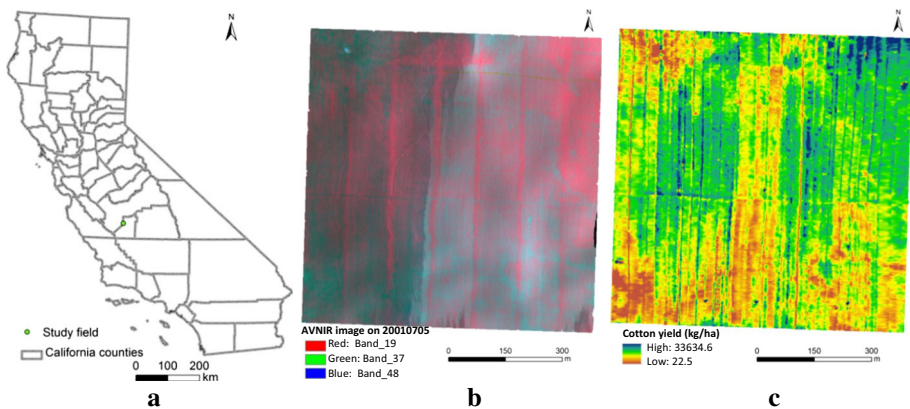


Fig. 1 The **a** approximate location of the study area in California, USA, **b** 5 July 2001 AVNIR image as a Color Infrared composite (bands at 833, 668, 552 nm), and **c** cotton harvester yield map of the study field

Table 1 Dates and days after planting (DAP) of acquired airborne hyperspectral images

Date	June	July				August			September		October	
	20	5	11	25	31	8	21	28	5	27	11	17
DAP	66	81	87	101	107	115	128	135	143	165	179	185

Cotton yield and management data collection

Yield data were collected using a cotton yield monitor on-board the harvester with yield accuracy estimated from 95 to 98% for pixels of approximately 4.5 m by 4.5 m (Zarco-Tejada et al. 2005). The harvester map in Fig. 1c reveals the spatial variability of yield. In addition to yield data, the grower provided detailed information on farming practices, including fertilizer and irrigation schedules. Fertilizer recommendations were based on soil and petiole sampling, and a single fertilizer rate was applied to the entire field (Zarco-Tejada et al. 2005). Shortly after the initial cotyledons formed (approximately DAP 66), the first irrigation was applied by sprinkler. Furrow irrigation was used to minimize water stress, with repeat irrigation every 2–3 weeks depending on the outcomes of frequently monitored leaf water potential. The sprinkler irrigation was applied only once near the beginning of the growing season on 20 June, and the last furrow irrigation was 18 August. After the last irrigation, the plants were allowed to dry before the September application of harvest-aid chemicals (leaf defoliant and desiccant) for the 21 October 2001 harvest (Zarco-Tejada et al. 2005).

VI calculations

Zarco-Tejada et al. (2005) evaluated 34 spectral VIs, including indices related to structure (10), chlorophyll (7), water (3), red edge fitting parameters (5) and combination indices (9) by calculating the correlation coefficients (r) between VI values and yield data within each pixel for 12 image dates. Their results demonstrated that the structural indices related to LAI (e.g. Normalized Difference Vegetation Index (NDVI; (Rouse and Deering 1973), Optimized Soil-Adjusted Vegetation Index (OSAVI; (Rondeaux et al. 1996), Renormalized Difference Vegetation Index (Roujean and Breon 1995) and Modified Triangular Vegetation Index (Haboudane et al. 2004)) were more strongly correlated to yield than the other indices. For this study, NDVI and OSAVI were chosen; NDVI because it is the most widely used vegetation index, and OSAVI for the ability to evenly distribute soil residual error across the entire range of crop fractional coverage levels (Steven 1998). In addition, this study evaluated the first and second derivatives (ρ' , ρ'') calculated from the pixel spectra.

As most remote sensing images are multispectral, to make the study result generally applicable, multispectral indices (NDVI and OSAVI) were calculated from reflectance at narrow bands of 668 and 833 nm (Eqs. 1, 2) using Band-Math in ENVI 4.8 (EXELIS, McLean, VA, USA), as these bands are close to the center of Landsat TM/ETM bands 3 and 4. The hyperspectral indices (ρ' and ρ'') were calculated over all 60 bands with an IDL program (Gorodetzky 2002), as there are dozens of ρ' and ρ'' over all the bands, the correlation between yield and ρ' , ρ'' were calculated to determine the most significant ρ' and ρ'' , then ρ' and ρ'' at 717 nm were used for SSMZ delineation.

$$\text{NDVI} = (\rho_{833} - \rho_{668}) / (\rho_{833} + \rho_{668}) \quad (1)$$

$$\text{OSAVI} = (1 + 0.16) \times (\rho_{833} - \rho_{668}) / (\rho_{833} + \rho_{668} + 0.16) \quad (2)$$

$$\text{1st Derivative}_\lambda = (\rho_{\lambda+1} - \rho_{\lambda-1}) / 2\Delta\lambda \quad (3)$$

$$\text{2nd Derivative}_\lambda = (\rho'_{\lambda+1} - \rho'_{\lambda-1}) / 2\Delta\lambda \quad (4)$$

where, ρ is reflectance value and λ is the wavelength of hyperspectral band.

Principles of OO segmentation

Farming practices and environmental studies are often conducted not on individual pixels, but on defined zones, such as SSMZs with relatively homogeneous crop growth and soil conditions. These real objects are derived statistically by clustering individual pixels into uniform regions (objects) within images and yield maps (Fig. 1b, c) using a multi-spatial resolution segmentation algorithm developed by Tian and Chen (2007) and Baatz et al. (2004). The size of object aggregation is controlled by the scale, which “describes the magnitude or the level of aggregation (and abstraction) on which a certain phenomenon can be described” (Baatz et al. 2004; Benz et al. 2004). Larger scale delineated larger real objects. This algorithm minimizes the heterogeneity among image objects, weighted by their size and shape, during the aggregation process. The iterative process starts with single pixels and merges them with surrounding single pixels into homogeneous objects. Succeeding iterations combine ever-increasing numbers of similar pixels into existing objects. Merges are performed in a pairwise manner. For each possible merge of two adjacent objects, the heterogeneity change is quantitatively compared with the overall change in heterogeneity ($\Delta h_{\text{overall}}$, defined in Eq. 5). A possible merge is fulfilled if the change in heterogeneity is less than the specified threshold (Tian and Chen 2007). Hence, larger threshold values allow for more pixel merges, and lead to larger objects.

For this SSMZ classification, the algorithm described by Baatz et al. (2004) and Benz et al. (2004) was adopted to calculate the heterogeneity and shape changes after merging spectral values among pixels either within a single VI image or time series of VI images. For a possible merge of any pair of adjacent SSMZs, an overall heterogeneity change was calculated with Eq. (5):

$$\Delta h_{\text{overall}} = (1 - W_{\text{shape}}) \Delta h_{\text{VI}} + W_{\text{shape}} \Delta h_{\text{shape}} \quad (5)$$

where W_{shape} is an assigned weight of importance ranging from 0 to 1. Δh_{VI} and Δh_{shape} measure the heterogeneity changes of VI and shape, respectively, and are defined as follows:

$$\Delta h_{\text{VI}} = \sum_{i=1}^N W_i \left(n_{\text{Merge}} \sigma_i^{\text{Merge}} - (n_{\text{SSMZ1}} \sigma_i^{\text{SSMZ1}} + n_{\text{SSMZ2}} \sigma_i^{\text{SSMZ2}}) \right) \quad (6)$$

$$\Delta h_{\text{shape}} = W_{\text{cmpct}} \Delta h_{\text{cmpct}} + (1 - W_{\text{cmpct}}) \Delta h_{\text{smooth}} \quad (7)$$

where N denotes the number of image VI layers, W_i represents the weight assigned to the i th VI layer and n denotes the number of pixels belonging to the potential Merge and existing SSMZ1 and SSMZ2 objects. The terms σ_i^{SSMZ1} , σ_i^{SSMZ2} and σ_i^{Merge} represent respective standard deviations within VI values from pixels existing and potentially merged (Eq. 6).

Baatz et al. (2004) and Benz et al. (2004) also defined the measures Δh_{cmpct} and Δh_{smooth} , which are obtained in a comparative manner illustrated by Eqs. (8) and (9).

$$\Delta h_{\text{cmpct}} = n_{\text{Merge}} \frac{l_{\text{Merge}}}{\sqrt{n_{\text{Merge}}}} - \left(n_{\text{SSMZ1}} \frac{l_{\text{SSMZ1}}}{\sqrt{n_{\text{SSMZ1}}}} + n_{\text{SSMZ2}} \frac{l_{\text{SSMZ2}}}{\sqrt{n_{\text{SSMZ2}}}} \right) \quad (8)$$

$$\Delta h_{\text{smooth}} = n_{\text{Merge}} \frac{l_{\text{Merge}}}{\sqrt{n_{\text{Merge}}}} - \left(n_{\text{SSMZ1}} \frac{l_{\text{SSMZ1}}}{\sqrt{n_{\text{SSMZ1}}}} + n_{\text{SSMZ2}} \frac{l_{\text{SSMZ2}}}{\sqrt{n_{\text{SSMZ2}}}} \right) \quad (9)$$

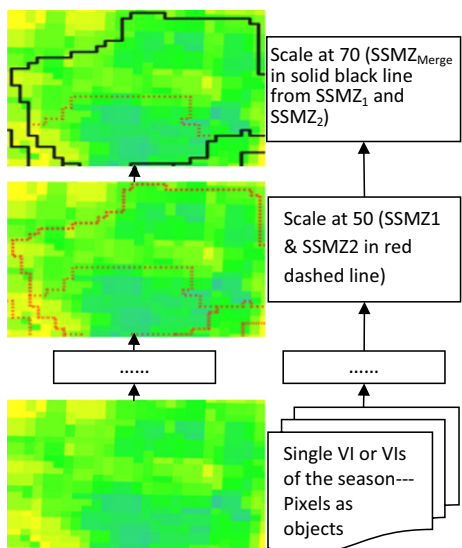
where l^{SSMZ1} , l^{SSMZ2} and l^{Merge} represent perimeter of the potential Merge and existing SSMZ1 and SSMZ2 objects. b^{SSMZ1} , b^{SSMZ2} and b^{Merge} represent perimeter of the potential Merge and existing SSMZ1 and SSMZ2 objects' bounding box.

The protocols described above ensure a steady and unique segmentation result given a certain set of the parameters (scale, W_{shape} and W_{cmpct}) for an image (Tian and Chen 2007). Equation (5) through (9) govern the local computation and decision-making for all the possible pairwise merges. An example of multi-spatial resolution segmentation for SSMZs is shown in Fig. 2.

SSMZ segmentation

Essential parameters, including input VI layers, scale, W_{shape} and W_{cmpct} , were used to derive the ideal SSMZ segmentation for farm practice efficiency. This study used the multi-spatial resolution segmentation algorithm embedded in the OO software eCognition (Trimble Geospatial Imaging, Sunnyvale, CA, USA). After transforming each AVNIR image to VI and derivative images, the images were stacked into individual VI images as bands in date sequence. When the multi-spatial resolution segmentation algorithm was conducted on time series images, multi-temporal information was also taken into account for SSMZ delineation. The optimal input VI and scale were the two key parameters determined as being important for minimizing heterogeneity and maximizing the

Fig. 2 Multi-spatial resolution segmentation for SSMZs with vegetation indices from hyperspectral images



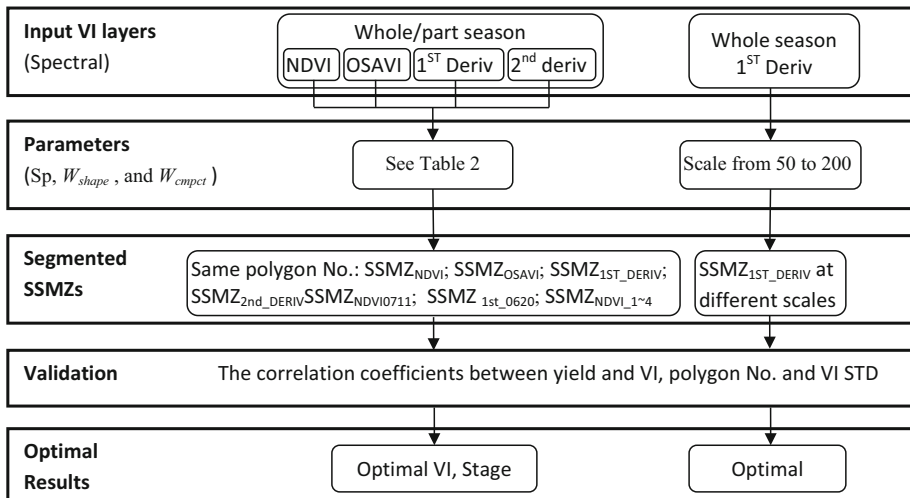


Fig. 3 SSMZ delineation vegetation indices from hyperspectral images and evaluation flowchart

compactness of SSMZ delineation. The SSMZ delineation and evaluation flowchart is shown in Fig. 3.

Methods to determine optimal VI

In determining the optimum input VI, each VI sequence image was segmented using a range of scales to create the same number of SSMZ objects for each and comparing the resulting zone maps. The names SSMZ_{NDVI}, SSMZ_{OSAVI}, SSMZ_{1ST_DERIV} and SSMZ_{2nd_DERIV} are the resulting segmented images using NDVI, OSAVI, ρ' and ρ'' image sequence for the entire season, respectively.

Methods to determine optimal scale

To evaluate the optimal scale, 12 first derivative input layers and a range of scales from 50 to 200 were used to segment the yield and VI images into various numbers and areas for SSMZs.

Methods to determine optimal date or accumulated dates

When the multi-spatial resolution segmentation algorithm was conducted on time series images, multi-temporal information were also taken into account for SSMZ delineation. To determine whether a single date or a portion of the season (cumulative VI values over a range of image dates) was most appropriate for delineating SSMZs, whether single or accumulated index values through sequential periods in the growing season, such as before boll development, would improve the correlation of VIs to yield was evaluated. VI image sequences of various durations were segmented, each correlation was calculated between yield and accumulations of VI values through an increasing number of dates from one to 12 dates (20 June–17 October). For example, NDVI on July 11, ρ' on June 20 and

accumulated NDVIs of the first four stages were used to segment SSMZs. These were named as $SSMZ_{NDVI0711}$, $SSMZ_{1st_0620}$ and $SSMZ_{NDVI_1 \sim 4}$, respectively.

Table 2 shows the parameters for site-specific management zones segmented with different methods listed above.

Quantitative criteria for SSMZ validation

Although image segmentation is a very important step, there are no established quantitative criteria to determine the best parameters for segmentation. Most studies have employed a qualitative visual inspection method (Chen et al. 2006). As quantitative criteria for this study, mean and standard deviation (STD) of VI were used as indicators of the relationship between the uniformity of crop growth and yield within each SSMZ. The correlation coefficients between mean yield and mean of VI within SSMZs (r_{VI_yield}), number of SSMZ polygons, standard deviation (STD) of VI and root mean square error (RMSE) of yield predicted by VI were calculated to determine the optimal VI, period within crop growth, and scale. Statistical tests were conducted in SPSS (IBM Inc., Chicago, IL, USA).

Results and analysis

Spatial variability in cotton growth

The variation of early cotton growth is visible in a color infrared (CIR) image (Fig. 1b) as tones of red and corresponding variation in NDVI values for 5 July 2001 image. This image is early in the season when substantial portions of the field were still bare soil. As determined from grower records, furrow irrigation in the field had already begun, and progress across the field can be seen in lower reflectance in areas of darker soil on the west side of the field (left side of the CIR image). Also visible is the pattern of several crop rows

Table 2 Parameters for site specific management zones segmented using different VIs vegetation indices derived from hyperspectral images

	Stage	Scale	Shape weight	Compactness	Polygon number	R_{VI_yield}	RMSE
$SSMZ_{NDVI}$	Whole season	3.39	0.0001	0.5	243	0.850	298.760
$SSMZ_{OSAVI}$	Whole season	3.63	0.0001	0.5	243	0.850	300.226
$SSMZ_{1ST_DERIV}$	Whole season	107	0.1	0.5	243	0.861	290.043
$SSMZ_{2nd_DERIV}$	Whole season	65	0.1	0.5	243	0.690	382.896
$SSMZ_{NDVI0711}$	July 11	4.51	0.002	0.5	243	0.872	289.642
$SSMZ_{1st_0620}$	June 20	105	0.0001	0.5	243	0.852	298.428
$SSMZ_{NDVI_1 \sim 4}$	First 4 dates	4.02	0.001	0.5	243	0.876	273.713

R_{VI_yield} is the correlation coefficients between the mean yield and mean of VI within SSMZs. All R_{VI_yield} values are significant at the 0.01 level (2-tailed). NDVI, OSAVI, 1ST_DERIV AND 2nd_DERIV are multispectral and hyperspectral indices

in a north–south direction which had greater plant growth due to an earlier sprinkler irrigation application. This higher growth rate persisted through the growing season, and the overall spatial pattern seen in the yield map (Fig. 1c) is similar to vegetation and soil distributions (Fig. 1b). Cotton spectra were extracted from various pixels within the 11 July AVNIR image (Fig. 4) to represent different growth conditions based on variation in NDVI values (Fig. 5), and both figures show significant spatial and spectral heterogeneity for potential SSMZs. S1 in Fig. 4 shows the spectral curve of pixels with the lowest cotton vegetation cover, which is cyan in Fig. 5, while S6 shows that of pixels with the highest cotton cover, which is red in Fig. 5; there is increasing cotton vegetation cover from S1 to S6.

Four bands for VI construction, namely 668, 716, 736 and 833 nm, are marked on Fig. 4. The first and second derivative values were derived at band 726 nm by using reflectance values at 716 and 736 nm, and found to be strongly correlated with cotton yield. Note in Fig. 4 that the 726 nm position was slightly greater than the inflection point along the red edge and corresponds to earlier findings regarding plant reflectance.

SSMZ segmentation results

The scale (Ψ), shape weight (W_{shape}) and compactness weight (W_{compact}) parameters used to select the most effective VI are shown in Table 2. SSMZs segmented from NDVI ($\text{SSMZ}_{\text{NDVI}}$) and first derivative ($\text{SSMZ}_{\text{1ST_DERIV}}$) images at scale 107 are portrayed in Fig. 5 with the 11 July 2001 AVNIR image as the background. At this scale, $\text{SSMZ}_{\text{NDVI}}$ and $\text{SSMZ}_{\text{1ST_DERIV}}$ separate into 243 polygons. The boundary of each SSMZ follows the spatial variation within cotton CIR composition, and appears to delineate areas of similar, uniform image color within each SSMZ object. In Fig. 5, $\text{SSMZ}_{\text{1ST_DERIV}}$ describes more detail in spatial variation compared to $\text{SSMZ}_{\text{NDVI}}$, and appears to be more easily influenced

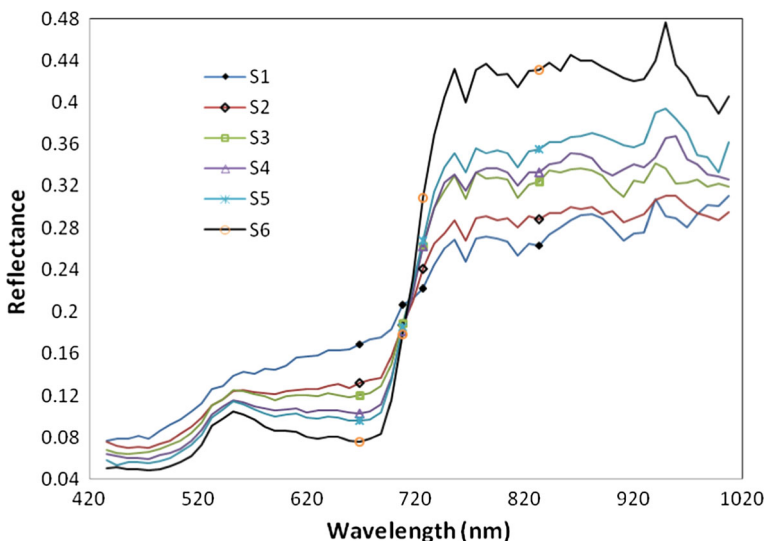


Fig. 4 Spectra (S1, S2, etc.) for various amounts of cotton cover densities in pixels extracted from July 11, 2001 AVNIR imagery

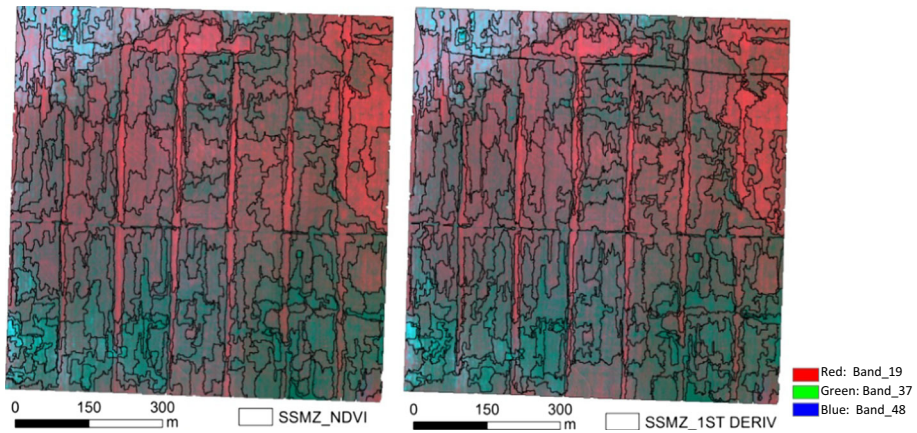


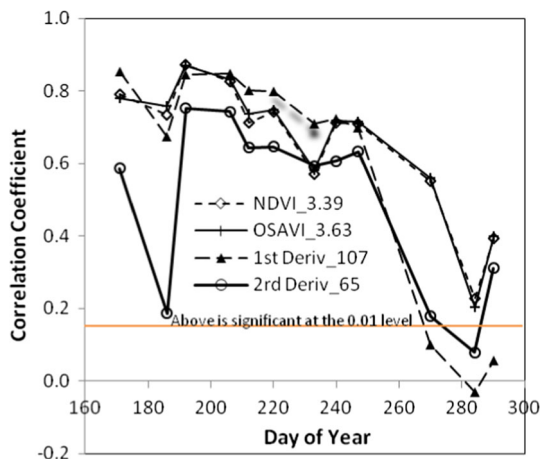
Fig. 5 SSMZs segmented with NDVI and 1st derivative (scale 107) overlaid on an AVNIR image (July 11, 2001) with color composite of band centers at 552, 668, and 833 nm

by canopy variation. The objects also appear to follow soil and irrigation spatial patterns. For the same scale, SSMZ objects from different VIs have similar spatial patterns.

Optimal VI for SSMZ delineation

To determine the optimal VI for SSMZ delineation, image maps for each VI and image date throughout the season were segmented into SSMZs with the same number of objects in a sequence of eight scale values. Results for VIs NDVI ($SSMZ_{NDVI}$), OSAVI ($SSMZ_{OSAVI}$), and first and second derivatives ($SSMZ_{1ST_DERIV}$ and $SSMZ_{2nd_DERIV}$) are shown in Table 2 with associated number of SSMZ objects, mean yield standard deviation values within the SSMZs, Pearson's correlation coefficient for VI to yield values (r_{VI_yield}) and RMSE of yield predicted by VI. As larger correlation coefficients match to smaller RMSE values for all VI SSMZ results, only correlation coefficient is discussed. The correlation coefficients between mean cotton yield and VI within SSMZ objects on each

Fig. 6 Correlation coefficients between mean cotton yield and VIs within SSMZ objects derived from time-series vegetation indices [All correlation coefficients are significant at the 0.01 level (2-tailed)]



date are also plotted in Fig. 6 (“NDVI_3.39” means that SSMZs were segmented from NDVI images at the scale of 3.39; other numbers in Fig. 6 legend are also scale values). All correlation coefficients shown in Table 2 and Fig. 6 are significant at the 0.01 level (2-tailed), except for the last three dates after DAP 143 in Fig. 6. (Zarco-Tejada et al. 2005) listed the correlation strength varied during the cotton growing season. All results from VI segmenting show strong correlations between mean cotton yield and VIs before DAP 165 (27 September) and irrigation cut off. The strength of correlation between yield and VIs within SSMZs increases with increasing cotton growth beginning DAP 66 (20 June) to maximum correlation coefficients for DAP 87(11 July image) with NDVI and OSAVI. While NDVI, OSAVI and first derivative indices remained well correlated during this period, the correlation of the second derivative is less significant. (Zarco-Tejada et al. 2005) reported a similar trend in correlations for pixel based analysis. Results showed that at the beginning of the season, first derivatives and NDVI and OSAVI, while remaining asymptotic to LAI, were better for SSMZ delineation. NDVI and OSAVI had the most significant correlation with cotton yield on DAP 87 (11 July), and the first derivative was more consistent during the mid-growing season from DAP 101 (July 25) to DAP 135 (Aug. 28), may be considered better for periods with high crop biomass. Although too late for altering management practices during senescence, NDVI and OSAVI remained significantly correlated to yield, and a higher correlation coefficient than the poor performance of first and second derivative indices. These results underscore that selecting the optimal VI for a given scale of SSMZ delineation may depend on the period within the cotton growing season.

Optimal stage for SSMZ delineation

The specific image date NDVI, OSAVI, and first derivative indices values with the best correlation strength to yield were segmented into SSMZs. Some example data, including correlation to yield, as well as the input segmentation parameters for these are shown in Table 2 for NDVI on DAP 87(11 July; SSMZ_{NDVI0711}) and first derivative on DAP 66 (20 June; SSMZ_{first_0620}). The correlation coefficients to yield among SSMZs between segmentation using SSMZ_{NDVI0711} and SSMZ_{1st_0620} are 0.87 and 0.85, respectively. This finding indicates different DAPs were optimal for SSMZ delineation, depending on VI, although both of these indices were optimum early in the growing season. This information may be early enough for a grower to modify irrigation and other practices.

Accumulated VI through sequential periods for SSMZ delineation

In respect to plant growth, the best correlation coefficients of accumulated VI values for NDVI and OSAVI occurred with the fourth starting date accumulation of DAP from 66 through 101 (image date 20 June to 25 July). This accumulated NDVI correlation coefficient ($r = 0.88$) was similar to the best single date NDVI correlation coefficient ($r = 0.87$) from DAP 87 (11 July) in the four images accumulated. The accumulated and single date OSAVI correlation coefficients were similar to those of NDVI. Similar correlation to yield for the same period were achieved using the accumulation of first derivative images ($r = 0.87$), and nearly the same correlation for the best single image first derivative correlation for the season ($r = 0.86$).

Optimal scale for SSMZ delineation

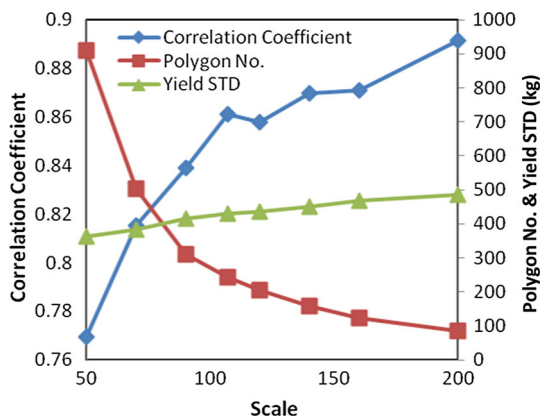
While the scale is likely to be set by grower management precision requirements, the interaction of SSMZ delineation scale and VIs relationship to yield was evaluated. Using a range of scales from 50 to 200, first derivative layers for the entire season were delineated into SSMZ. The influence of SSMZ delineation scale on (i) number of SSMZ objects, (ii) correlation coefficients between means of VI and yield within objects, and (iii) mean STD of yield recorded within delineated SSMZ objects is shown in Fig. 7. Note that beyond the mid-point towards the scale of 200, the decline in the number of objects slows, measured yield STD slightly flattens and correlation coefficient values improve only slightly. These curves indicate a median point between large easily managed objects and increased resource efficiency in site-specific farming applications. As Fig. 7 suggests, an optimal scale for this field SSMZ delineation when using a first derivative index was approximately 107 at the inflection points (points of diminishing returns) for the three criteria, and created approximately 240 SSMZ objects. While all SSMZs across these scales described the spatial variation of crop growth well with correlation coefficients above 0.77, fewer and larger objects may be better for site specific application strategies.

Discussion

The physico-chemical properties of soil and crops demonstrate considerable spatial variability in heterogeneity, which cannot be described solely on the basis of individual imagery pixels. Precision agriculture and site-specific farming are also not conducted at the pixel level, so OO segmentation with single or a sequence of VI images as input layers allowed the determination and evaluation of SSMZ delineation, taking relatively uniform crop growth and stress areas as objects. This approach could improve the performance of precision agriculture and site-specific farming practices.

Since the spectral, spatial and temporal information all contribute to the sequence of hyperspectral images, the OO SSMZ delineation method may be less sensitive to noise introduced from multi-resource data. There were errors in the yield map because of the low spatial resolution of GPS receivers and yield monitors on machinery, which can be seen from the abnormalities along some columns in the yield map (Fig. 1c). The geometric and

Fig. 7 Number of SSMZ polygons and standard deviation of yield, and correlation coefficient between yield and accumulated 1st derivative [correlation is significant at the 0.01 level (2-tailed)]



atmospheric correction process for airborne images also inevitably resulted in errors (shown in Fig. 1b). These errors may have influenced the relationship between VI and cotton yield. However, since the OO segmentation created SSMZ polygons consisting of hundreds of pixels, the influence of abnormal data was diminished and the relationship between VI and yield maintained a strong correlation. Similarly, high correlation with various sequences of VI and derivative images indicates less sensitivity to timing. An OO map used to create SSMZ during early and mid-season shows greater strength, rather than later in the season. However, for this set of imagery and yield, cumulative VI values for part or entire seasons may only provide redundant information given the resulting correlation values in NDVI, OSAVI and first derivative from a single early date.

Mean NDVI and OSAVI values within SSMZs were highly correlated to yield, indicating that multispectral imagery may also be satisfactory for SSMZ segmentation. Since multi-band satellite imagery is readily available, less expensive, and often more frequent, it may be worthwhile acquiring data from early in the growing season, even in previous seasons, to investigate SSMZs with OO segmentation.

Homogeneous SSMZ objects improved the correlation to yield compared to single pixels. The correlation between VI and yield are greater than the pixel-based correlation results calculated by Zarco-Tejada et al. (2005). Segmented OO results follow the nature of SSMZs in that spectrally similar and contiguous pixels are grouped as SSMZs. In addition, segmentation scale provides greater control in defining the number (and thus size) of spatial units, which can be tailored to the needs of field management practices. In addition to spectral information, image objects may be segmented using additional layers of attributes such as micro-climate and geophysical conditions. In this study, only image VI values were used to define the mean and STD values within SSMZ objects.

Senay et al. (1998) used only one airborne multispectral image at the end of the growing season (15 September 1994) for delineating site-specific farming zones. Boydell and McBratney (2002) identified potential within-field management zones from cotton yield estimates with a single mid-season Landsat TM in each of 11 years. This study showed that the most significant correlations between yield and single date spectral index values occurred earlier in the growing season (Fig. 6).

The optimal scale determined in section “SSMZ segmentation” and shown in section “Accumulated VI through sequential periods for SSMZ delineation” is the theoretical optimal scale based on the number of SSMZ polygons, standard deviation of yield and correlation coefficient between yield and VI for coincident yield and image pixels. For practical application, scale should relate to the spatial resolution of site-specific practices and equipment, such as requirements for larger or smaller management areas due to differences in sprinkler distances, or widths of fertilizer injector and pesticide spray rigs. With the relationship of VI to crop growth, SSMZ objects can be segmented at different scales to generate practical SSMZs for different site-specific application purposes. For a specified area, larger-scale OO analysis delineates SSMZs of greater size and fewer in number, which is good for coarse site-specific management practices. Smaller scale OO analysis generates more detailed SSMZs, which may be better for more accurate site-specific management implementation, but will require more expensive and precise variable rate equipment.

OO segmentation partitions the data into SSMZs, not classes. As the zones are contiguous, they are manageable units for agricultural practices. Conversely, as OO segmentation does not produce classes, the zones have to be labelled according to a treatment class. Similar to the Effective Zone concept introduced by Pedroso et al. (2010), the application of OO segmentation to an auxiliary variable (multispectral and hyperspectral

VI_s) proved effective with a spatial constraint at partitioning the variance in a correlated but independent variable of agronomic interest (yield).

SSMZ and RS observations provide accurate input information for agricultural decision support systems (DSS) and site-specific farming practices. These technologies improve the capacity and accuracy of DSS and agronomic models by providing accurate input information and model validation data. Further investigations are needed with other crops, soils, climate and years to verify the findings of this study.

Conclusions

In this study, a new SSMZ delineation method based on the Object Oriented (OO) method was proposed and investigated using image sequences, optimal VI_s, scale and image dates. The SSMZs defined with the OO method at various scales improved the description of the spatial variation of yield within a cotton field, because much more significant correlations exist between yield and VI_s within SSMZs than that between yield and VI_s at pixel level. The optimal VI for SSMZ delineation was determined at the same scale, and VI relationship to yield demonstrated a dependence on image acquisition date during the growing season. Early in the season, when LAI is low, NDVI, OSAVI and first derivative indices were better for SSMZ delineation; during mid-season, with greater crop biomass, first derivative indices were better and, at end of the season, during crop senescence stages, NDVI and OSAVI were better performers. For regions with climate and irrigation patterns similar to this study area, it appears to be best to choose multispectral and hyperspectral images from early in the growing season to delineate SSMZs. However, as the results are based on a specific field and year, more work is needed to establish the generality of these results.

Acknowledgements The research was supported by the Program for new century excellent talents in Heilongjiang Provincial University, PRC, Postdoctoral start-up fund of Heilongjiang province (LBH-Q13026) and “Young Talents” Project of Northeast Agricultural University, PRC (14QC28). The study was conducted while the primary author was located at the University of California Davis.

References

- Baatz, M., Benz, U., Dehghani, S., Heynen, M., Höltje, A., Hofmann, P., et al. (2004). *eCognition professional user guide 4*. Munich, Germany: Definiens Imaging.
- Ben-Dor, E., Chabrilat, S., Dematté, J. A. M., Taylor, G. R., Hill, J., Whiting, M. L., et al. (2009). Using imaging spectroscopy to study soil properties. *Remote Sensing of Environment*, 113(Supplement 1(0)), S38–S55. doi:[10.1016/j.rse.2008.09.019](https://doi.org/10.1016/j.rse.2008.09.019).
- Benz, U. C., Hofmann, P., Willhauck, G., Lingenfelder, I., & Heynen, M. (2004). Multi-resolution, object-oriented fuzzy analysis of remote sensing data for GIS-ready information. *ISPRS Journal of Photogrammetry and Remote Sensing*, 58(3–4), 239–258. doi:[10.1016/j.isprsjprs.2003.10.002](https://doi.org/10.1016/j.isprsjprs.2003.10.002).
- Blaschke, T., & Strobl, J. (2001). What’s wrong with pixels? Some recent developments interfacing remote sensing and GIS. *GeoBIT/GIS*, 6(1), 12–17.
- Boydell, B., & McBratney, A. B. (2002). Identifying potential within-field management zones from cotton-yield estimates. *Precision Agriculture*, 3(1), 9–23. doi:[10.1023/a:1013318002609](https://doi.org/10.1023/a:1013318002609).
- Chen, Z., Zhao, Z., Gong, P., & Zeng, B. (2006). A new process for the segmentation of high resolution remote sensing imagery. *International Journal of Remote Sensing*, 27(22), 4991–5001.
- Davatgar, N., Neishabouri, M. R., & Sepaskhah, A. R. (2012). Delineation of site specific nutrient management zones for a paddy cultivated area based on soil fertility using fuzzy clustering. *Geoderma*, 173–174, 111–118. doi:[10.1016/j.geoderma.2011.12.005](https://doi.org/10.1016/j.geoderma.2011.12.005).

- De Benedetto, D., Castrignanò, A., Rinaldi, M., Ruggieri, S., Santoro, F., Figorito, B., et al. (2013). An approach for delineating homogeneous zones by using multi-sensor data. *Geoderma*, 199, 117–127. doi:[10.1016/j.geoderma.2012.08.028](https://doi.org/10.1016/j.geoderma.2012.08.028).
- Diker, K., Heermann, D., & Brodahl, M. (2004). Frequency analysis of yield for delineating yield response zones. *Precision Agriculture*, 5(5), 435–444.
- Franzen, D. W., Hopkins, D. H., Sweeney, M. D., Ulmer, M. K., & Halvorson, A. D. (2002). Evaluation of soil survey scale for zone development of site-specific nitrogen management. *Agronomy Journal*, 94(2), 381–389. doi:[10.2134/agronj2002.3810](https://doi.org/10.2134/agronj2002.3810).
- Gamanya, R., De Maeyer, P., & De Dapper, M. (2009). Object-oriented change detection for the city of Harare Zimbabwe. *Expert Systems with Applications*, 36(1), 571–588. doi:[10.1016/j.eswa.2007.09.067](https://doi.org/10.1016/j.eswa.2007.09.067).
- Gorodetzky, D. (2002). spectral_derivative.sav. (pp. CODE LIBRARY). Retrieved January 17, 2017, from <http://www.harrisgeospatial.com/>.
- Guastaferro, F., Castrignanò, A., Benedetto, D., Solitto, D., Troccoli, A., & Cafarelli, B. (2010). A comparison of different algorithms for the delineation of management zones. *Precision Agriculture*, 11(6), 600–620. doi:[10.1007/s11119-010-9183-4](https://doi.org/10.1007/s11119-010-9183-4).
- Haboudane, D., Miller, J. R., Pattey, E., Zarco-Tejada, P. J., & Strachan, I. B. (2004). Hyperspectral vegetation indices and novel algorithms for predicting green LAI of crop canopies: Modeling and validation in the context of precision agriculture. *Remote Sensing of Environment*, 90(3), 337–352.
- Hbirkou, C., Pätzold, S., Mahlein, A.-K., & Welp, G. (2012). Airborne hyperspectral imaging of spatial soil organic carbon heterogeneity at the field-scale. *Geoderma*, 175–176, 21–28. doi:[10.1016/j.geoderma.2012.01.017](https://doi.org/10.1016/j.geoderma.2012.01.017).
- Johansen, K., Coops, N. C., Gergel, S. E., & Stange, Y. (2007). Application of high spatial resolution satellite imagery for riparian and forest ecosystem classification. *Remote Sensing of Environment*, 110(1), 29–44.
- Johnson, C. K., Mortensen, D. A., Wienhold, B. J., Shanahan, J. F., & Doran, J. W. (2003). Site-specific management zones based on soil electrical conductivity in a semiarid cropping system. *Agronomy Journal*, 95(2), 303–315. doi:[10.2134/agronj2003.3030](https://doi.org/10.2134/agronj2003.3030).
- Lan, Y., Thomson, S. J., Huang, Y., Hoffmann, W. C., & Zhang, H. (2010). Current status and future directions of precision aerial application for site-specific crop management in the USA. *Computers and Electronics in Agriculture*, 74(1), 34–38. doi:[10.1016/j.compag.2010.07.001](https://doi.org/10.1016/j.compag.2010.07.001).
- Li, Y., Shi, Z., Li, F., & Li, H. Y. (2007). Delineation of site-specific management zones using fuzzy clustering analysis in a coastal saline land. *Computers and Electronics in Agriculture*, 56(2), 174–186.
- Liu, J. G., Miller, J. R., Haboudane, D., Pattey, E., & Nolin, M. C. (2005). Variability of seasonal CASI image data products and potential application for management zone delineation for precision agriculture. *Canadian Journal of Remote Sensing*, 31(5), 400–411.
- López-Lozano, R., Casterad, M. A., & Herrero, J. (2010). Site-specific management units in a commercial maize plot delineated using very high resolution remote sensing and soil properties mapping. *Computers and Electronics in Agriculture*, 73(2), 219–229. doi:[10.1016/j.compag.2010.04.011](https://doi.org/10.1016/j.compag.2010.04.011).
- McBratney, A., Mendonça Santos, M. D. I., & Minasny, B. (2003). On digital soil mapping. *Geoderma*, 117(1), 3–52.
- Moral, F. J., Terrón, J. M., & Da Silva, J. M. (2010). Delineation of management zones using mobile measurements of soil apparent electrical conductivity and multivariate geostatistical techniques. *Soil and Tillage Research*, 106(2), 335–343.
- Moran, M. S., Inoue, Y., & Barnes, E. M. (1997). Opportunities and limitations for image-based remote sensing in precision crop management. *Remote Sensing of Environment*, 61(3), 319–346. doi:[10.1016/S0034-4257\(97\)00045-X](https://doi.org/10.1016/S0034-4257(97)00045-X).
- Ouyang, Z.-T., Zhang, M.-Q., Xie, X., Shen, Q., Guo, H.-Q., & Zhao, B. (2011). A comparison of pixel-based and object-oriented approaches to VHR imagery for mapping saltmarsh plants. *Ecological Informatics*, 6(2), 136–146. doi:[10.1016/j.ecoinf.2011.01.002](https://doi.org/10.1016/j.ecoinf.2011.01.002).
- Pedroso, M., Taylor, J., Tisseyre, B., Charnomordic, B., & Guillaume, S. (2010). A segmentation algorithm for the delineation of agricultural management zones. *Computers and Electronics in Agriculture*, 70(1), 199–208. doi:[10.1016/j.compag.2009.10.007](https://doi.org/10.1016/j.compag.2009.10.007).
- Rondeaux, G., Steven, M., & Baret, F. (1996). Optimization of soil-adjusted vegetation indices. *Remote Sensing of Environment*, 55(2), 95–107.
- Roujean, J.-L., & Breon, F.-M. (1995). Estimating PAR absorbed by vegetation from bidirectional reflectance measurements. *Remote Sensing of Environment*, 51(3), 375–384.
- Rouse, J. W., R. H. Haas, J. A. Schell, & Deering, D. W. (1973). Monitoring vegetation systems in the Great Plains with ERTS. In *Third ERTS Symposium*, 1973 (pp. 309–317): NASA SP-351 I.

- Scudiero, E., Teatini, P., Corwin, D. L., Deiana, R., Berti, A., & Morari, F. (2013). Delineation of site-specific management units in a saline region at the Venice Lagoon margin, Italy, using soil reflectance and apparent electrical conductivity. *Computers and electronics in agriculture*, 99, 54–64.
- Senay, G., Ward, A., Lyon, J., Fausey, N., & Nokes, S. (1998). Manipulation of high spatial resolution aircraft remote sensing data for use in site-specific farming. *Transactions of the ASAE*, 41(2), 489–496.
- Simbahan, G., Dobermann, A., & Ping, J. (2004). Screening yield monitor data improves grain yield maps. *Agronomy Journal*, 96(4), 1091–1102.
- Steven, M. D. (1998). The sensitivity of the OSAVI vegetation index to observational parameters. *Remote Sensing of Environment*, 63(1), 49–60. doi:[10.1016/S0034-4257\(97\)00114-4](https://doi.org/10.1016/S0034-4257(97)00114-4).
- Tian, J., & Chen, D. M. (2007). Optimization in multi-scale segmentation of high-resolution satellite images for artificial feature recognition. *International Journal of Remote Sensing*, 28(20), 4625–4644.
- Uno, Y., Prasher, S., Lacroix, R., Goel, P., Karimi, Y., Viau, A., et al. (2005). Artificial neural networks to predict corn yield from compact airborne spectrographic imager data. *Computers and Electronics in Agriculture*, 47(2), 149–161.
- USDA-NRCS. (1978). Soil Survey Kings County, California. In U. N. R. C. Service (Ed.). Washington, DC, USA: USDA Soil conservation service U.S. Gov. Print.
- Van Coillie, F. M., Verbeke, L. P., & De Wulf, R. R. (2007). Feature selection by genetic algorithms in object-based classification of IKONOS imagery for forest mapping in Flanders Belgium. *Remote Sensing of Environment*, 110(4), 476–487.
- Yang, C., Everitt, J., Bradford, J., & Murden, D. (2009). Comparison of airborne multispectral and hyperspectral imagery for estimating grain sorghum yield. *Transactions of the ASABE*, 52(2), 641–649.
- Zarco-Tejada, P. J., Ustin, S. L., & Whiting, M. L. (2005). Temporal and spatial relationships between within-field yield variability in cotton and high-spatial hyperspectral remote sensing imagery. *Agronomy Journal*, 97(3), 641–653. doi:[10.2134/agronj2003.0257](https://doi.org/10.2134/agronj2003.0257).
- Zhang, N., Wang, M., & Wang, N. (2002). Precision agriculture—a worldwide overview. *Computers and Electronics in Agriculture*, 36(2–3), 113–132. doi:[10.1016/S0168-1699\(02\)00096-0](https://doi.org/10.1016/S0168-1699(02)00096-0).